The Astrophysical Journal, 612:364–374, 2004 September 1

GRAVITATIONAL WAVES FROM EXTRAGALACTIC INSPIRALING BINARIES: SELECTION EFFECTS AND EXPECTED DETECTION RATES

Philip Nutzman,[1] Vicky Kalogera,[1] Lee Samuel Finn,[2] Cy Hendrickson,[1] and Krzysztof Belczynski[1,3]
Received 2004 February 3; accepted 2004 May 12

ABSTRACT

We examine the selection effects that determine how the population of inspiraling binary compact objects (BCOs) is reflected by those potentially observed with ground-based interferometers like LIGO. We lay the groundwork for the interpretation of future observations in terms of constraints on the real population and, correspondingly, binary star evolution models. To determine the extragalactic population of inspiraling binaries, we combine data on distance and blue luminosity from galaxy catalogs with current models of the Galactic BCO mass distribution to simulate the physical distribution of binaries in the nearby universe. We use Monte Carlo methods to determine the fraction of binaries observable by the LIGO detectors from each galaxy as a function of the BCO chirp mass. We examine separately the role of source distance, sky position, time of detection, and binary system chirp mass on the detection efficiency and selection effects relevant to the three LIGO detectors. Finally, we discuss the implications of the nearby geography of space on anticipated gravitational wave detection and compare our results to those of previous studies, which have assumed uniform galaxy volume density and fixed chirp mass for BCOs. From these considerations, actual BCO inspiral observations or significant upper limits on the coalescence rate anticipated in the near future by ground-based interferometers can be used to improve our knowledge of the Galactic binary inspiral rate and to constrain models of radio pulsar characteristics and binary star evolution channels leading to neutron star or black hole binaries.

Subject headings: binaries: close — black hole physics — gravitational waves — stars: neutron

1. INTRODUCTION

Binary compact objects (BCOs) with neutron stars (NSs) or black holes (BHs) hold a special place among gravitational wave (GW) sources. The discovery of PSR B1913+16 (Hulse & Taylor 1974), the first binary pulsar system, inspired the detailed study of inspiraling compact binaries and provided the first observational evidence for the existence of gravitational radiation (Taylor & Weisberg 1989). Binary systems like PSR B1913+16 are driven to coalescence by a GW emission catastrophe: in the last approximately 20 s before they coalesce they radiate their remaining binding energy (approximately 2×10^{52} ergs) as GWs in a band accessible to large ground-based detectors like the Laser Interferometer Gravitational Wave Observatory (LIGO; Abbott et al. 2004a) and VIRGO (Caron et al. 1997).[4]

Current observational constraints on the population of NS or BH binary systems depend on radio pulsar observations of just a handful of Galactic binary systems (e.g., Burgay et al. 2004; Kalogera et al. 2004). In contrast, the LIGO and VIRGO detectors will observe stellar-mass inspiraling BCOs at extragalactic distances. They will also be sensitive to BH binaries, which are not observable electromagnetically. Correspondingly, observations by this new generation of detectors can help constrain the binary coalescence rate density in the nearby universe, and binary evolution models for the formation of such sources, in ways not possible with electromagnetic observations alone. In this work we begin laying the groundwork for the astrophysical interpretation of future GW observations of BCO inspirals by focusing attention on the selection effects associated with GW observations: in particular, effects associated with binary component masses, the GW antenna beam, and the local geography of the universe.

Over the past decade there have been many predictions of the detection rate for LIGO of BCO inspirals (e.g., Belczynski et al. 2002, hereafter BKB02; Kalogera et al. 2004). These calculations all begin by estimating the Galactic coalescence rate and extrapolating it to other galaxies. The observed rate is then calculated assuming that galaxies (and thus, binaries) are distributed homogeneously and isotropically in the local universe and that the LIGO detectors observe all coalescing binaries inside a fixed distance, which is the radius of a sphere that would have the same volume as is effectively surveyed by the detectors. These approximations are inadequate when we wish to go beyond order-of-magnitude predictions and actually interpret observed events as constraints on the actual BCO population, as is our goal.

To improve on past models for the physical population of inspiraling compact binary systems, we use galaxy catalogs to model the actual distribution of galaxies in the local universe, and we use stellar synthesis calculations (specifically, those of BKB02) to model the mass distribution of binaries within each galaxy. From the constructed population models, we determine the compact binary coalescence rate and distribution with binary system mass that we expect the LIGO detector system to observe, taking full account of each galaxy's distance and declination, the LIGO detector system's noise spectrum, and its position and orientation on Earth.

[1] Department of Physics and Astronomy, Northwestern University, 2145 Sheridan Road, Evanston, IL 60208; me@northwestern.edu, vicky@northwestern.edu, c-hendrickson@northwestern.edu, belczynski@northwestern.edu.

[2] Center for Gravitational Wave Physics, Pennsylvania State University, University Park, PA 16802; LSFinn@PSU.edu.

[3] Lindheimer Postdoctoral Fellow.

[4] Somewhat less energy will be radiated in the bands accessible to GEO (Abbott et al. 2004a) and TAMA (Ando et al. 2001), and less still in the bands accessible to the bar detectors AURIGA (Prodi et al. 1998), ALLEGRO (Mauceli et al. 1996), EXPLORER (Astone et al. 1993; Amaldi et al. 1986), and NAUTILUS (Astone et al. 1997).

Our principal goal in relating a physical population model to the distribution that we expect modern GW detectors to observe is to enable observations by those detectors to constrain the population model (see Bulik & Belczynski 2003 and Bulik et al. 2004 for recent studies with similar goals). Through the calculations described here, comparisons of future observed rates or rate upper limits constrain stellar synthesis models and the overall BCO population. While our principal interest is in preparing for this kind of interpretation of forthcoming observations, as a by-product of our investigations we have improved detection rate predictions as well.

In § 2 we present an overview of the various approaches used so far for the extrapolation of Galactic detection rates to extragalactic distances and introduce our novel galaxy-by-galaxy approach, whereby we calculate the detectability of BCO inspirals for each galaxy in our catalog. In § 3 we describe how we calculate, from the detailed extragalactic population model described in § 2, the observed distribution of BCOs. In § 4 we discuss our results, including the LIGO detector system's efficiency for detecting binaries from different galaxies in the nearby universe, the expected observed coalescing binary mass distribution, new detection rate predictions, and the implications of the geography of the nearby universe for detection of BCO systems. We end in § 5 with a summary of our main conclusions.

2. ESTIMATING THE BCO POPULATION DENSITY IN THE NEARBY UNIVERSE

Our final goal is to understand how the actual population and distribution of coalescing BCOs are mapped to GW observations by LIGO (or GEO, TAMA, or VIRGO) of inspiraling binary systems. The signal amplitude depends on the system's distance, location on the detector's sky, orbital plane inclination with respect to the detector's line of sight, and binary chirp mass (see eq. [5a]). In this section we characterize the BCO population distribution in space and component masses: i.e., the density as a function of distance, position on the detector's sky, and chirp mass.

2.1. *Previous Studies*

All studies of compact object coalescence GW detection rates begin with an estimate of the intrinsic coalescence in our own Galaxy. Two methods have been employed to derive these rates: statistical analysis of the observed sample of inspiraling binary candidates and theoretical investigations based on understanding of BCO formation. The first approach so far provides us with the best rate constraints (see Burgay et al. 2004 and Kalogera et al. 2004 for the most recent estimates, in view of a newly discovered NS-NS system), but it is still limited by a small observed sample (currently three systems), some uncertainty in the selection effects associated with, e.g., pulsar beaming and radio luminosity, and the absence of known BH-NS and BH-BH binaries. The second approach provides us with results for all types of BCOs based on binary population synthesis models, which are generally calibrated to match the empirical estimates of Type II supernova rates (Belczynski et al. 2002, hereafter BKB02, and references therein), but the uncertainties associated with binary evolution models are significant. At present, our best estimates of Galactic coalescence rates place them in the range of 10^{-5} to 10^{-3} yr^{-1} for NS-NS, 10^{-6} to 10^{-4} yr^{-1} for BH-NS, and 0 to 10^{-4} yr^{-1} for BH-BH binaries.

All extrapolations from Galactic rates to extragalactic rates are based on the assumption that the formation of BCOs in a region is proportional to the blue luminosity in that region, corrected for reddening (Phinney 1991). Correspondingly, the coalescence rate density $R_{\rm det}$ within a distance $D_{\rm max}$ is proportional to the Milky Way coalescence rate density $R_{\rm MW}$ and the ratio of the blue luminosity within the sphere to the Milky Way blue luminosity:

$$R_{\rm det} = \frac{\mathcal{L}_b}{L_{\rm MW}} \left(\frac{4}{3}\pi D_{\rm max}^3\right) R_{\rm MW}, \tag{1}$$

where $\mathcal{L}_b$ is the mean blue luminosity volume density within a distance $D_{\rm max}$, $L_{\rm MW}$ is the total blue luminosity of the Milky Way, and $R_{\rm MW}$ is the coalescence rate in the Milky Way. The distance $D_{\rm max}$ is calculated so that, if coalescing binaries with given component masses (e.g., 1.4 $M_\odot$) are assumed to be uniformly distributed throughout space with rate density $\dot{n}$, the rate of detections in a GW detector above a given signal-to-noise ratio is

$$\dot{N}_{\rm GW} = \frac{4\pi}{3} D_{\rm max}^3 \dot{n}; \tag{2}$$

i.e., $D_{\rm max}$ is the radius of a sphere whose volume is the effective volume surveyed by the detector for binary systems with these component masses (Finn 1996, 2001a; Kalogera et al. 2001).

2.2. *A Galaxy Catalog Approach*

Here we describe a method appropriate for extrapolating Galactic BCO coalescence rates beyond the galaxy, for the purpose of estimating inspiral detection rates in GW detectors. Our ultimate goal is not the prediction of what might be seen, but to understand how observed bounds on the coalescence rate, perhaps as a function of the BCO component masses determined from these observations, can inform our understanding of binary populations in galaxies and binary population synthesis. Toward that end we improve on the method of binary inspiral rate estimation, described in § 2.1, in three ways:

1. The blue luminosity scaling argument is accurate when the survey volume is so large that local fluctuations in the galaxy density and the blue luminosity per galaxy are small. This is not the case in the local universe, where the galaxy distribution is strongly anisotropic. To overcome this difficulty we make use of galaxy catalogs to map the true distribution of galaxies in space and in blue luminosity.
2. A detector's sensitivity is not isotropic: e.g., the detector is more sensitive to binaries immediately above and below the plane of its arms than to binaries in its plane. We take full account of the detector's actual beam and its orientation with respect to the sky, averaged over the sidereal day.
3. Estimates to date use a $D_{\rm max}$ chosen for a particular combination of component masses.[5] We estimate the inspiral detection rate for the theoretically expected distribution of component masses, as opposed to some canonical mass.

2.2.1. *Spatial Distribution of Galaxies*

Galaxies are distributed anisotropically in the local universe, and this affects the interpretation of BCO inspiral detection rates in terms of galactic populations of BCOs. To take into

[5] In previous surveys binaries are assumed to be either NS-NS, with component masses of 1.4 $M_\odot$, or BH-NS binaries, with component masses of 10 and 1.4 $M_\odot$.

account the nearby distribution of galaxies, we draw galaxy data from two catalogs: the Lyon-Meudon extragalactic database (LEDA; Paturel et al. 1989) and the Tully Nearby Galaxy Catalog (NBG; Tully 1988a, 1988b).[6] We select these galaxy data sources for their homogeneous coverage of the sky: GW detectors have some sensitivity to BCOs in every direction on the sky, and so data from surveys that cover only sectors of the sky, such as the Sloan Digital Sky Survey (York et al. 2000), are not adequate.

Our principal source of galaxy data is the LEDA. It is comprehensive for galaxies with blue magnitudes brighter than 14.5 and partially complete for those as faint as $m = 17$ (Paturel et al. 1989). Owing to the difficulties in determining galaxy distances, the LEDA lacks distance data for all but a small fraction of its galaxies. The NBG, on the other hand, has excellent information for galaxies with radial velocity less than 2500 km s^{-1} but makes no attempt to be comprehensive beyond that range (Tully 1988a, 1988b). In order to have available the best galactic distance estimates, we use the NBG distance data with the corresponding LEDA galaxies and derive distances for all other LEDA galaxies using the measured radial velocities and $H_0 = 70$ km s^{-1} Mpc^{-1}. Our synthesized catalog thus provides the needed parameters of right ascension α, declination δ, distance D, and blue luminosity corrected for reddening for each galaxy.

A primary concern with any galaxy catalog is incomplete coverage of faint galaxies. Our catalog is complete for galaxies brighter than blue magnitudes of 14.5; correspondingly, incompleteness is important for faint galaxies beyond approximately 20 Mpc and for galaxies of increasing intrinsic brightness at greater distances.

To compensate for the missing galaxies while still accounting for their nonuniform spatial distribution, we introduce a distance-dependent correction factor, which is the ratio of the expected blue luminosity, where the catalog is complete, to the blue luminosity reported by the catalog at each distance. To derive this factor we calculate the expected distribution of luminosity with distance, assuming that the true distribution with distance is proportional to the luminosity distribution at that distance for galaxies *brighter* than the completeness limit at each distance. Since our galaxy catalog is essentially complete with regard to cumulative blue luminosity up to approximately 22 Mpc, we calibrate the resulting distribution to match the cataloged distribution at this distance.

Figure 1 shows the corrected cumulative blue luminosity as a function of distance. For comparison, we also show the cumulative blue luminosity expected under the assumption of uniform blue luminosity density, as adopted in Kalogera et al. (2001). The normalization of the uniform blue luminosity density curve is based on galaxy surveys out to large distances. Three elements of this figure are worth noting in more detail. First, the uniform blue luminosity density approximation clearly underestimates the actual blue luminosity contributed by nearby galaxies. Second, the Virgo Cluster contributes to a large step in the cumulative blue luminosity at approximately 20 Mpc. The higher local blue luminosity density at this distance significantly increases the estimated detection rate as a fraction of the total number of coalescing systems, especially for initial detectors. Finally, beyond the Virgo Cluster the blue luminosity grows more slowly than the third power of distance (see § 4.5), as the local overabundance of galaxies blends into the homogeneous distribution at larger scales.

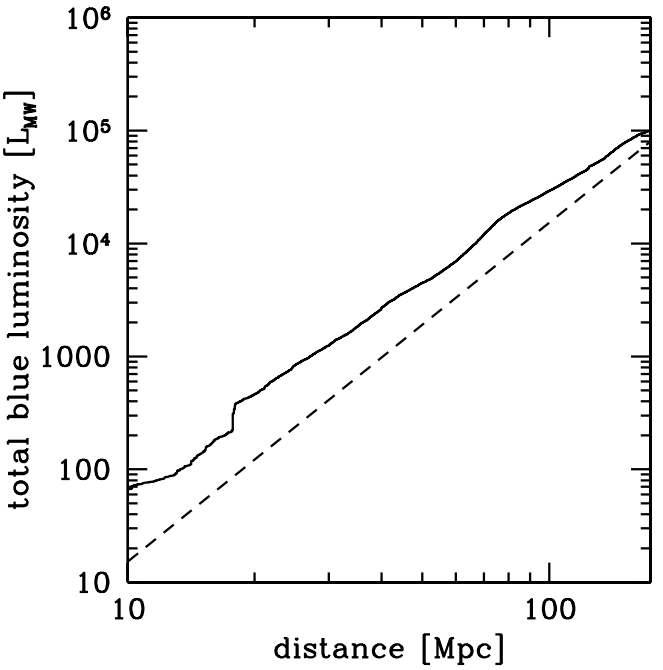

FIG. 1.—Cumulative blue luminosity enclosed within a distance D using the LEDA galaxy catalog and correcting for incompleteness. The dashed line is produced assuming a uniform distribution of luminosity in space (using the normalization density adopted in Kalogera et al. 2001).

An important assumption in our correction for completeness is that the spatial distribution of the missing luminosity follows the spatial distribution of the recorded galaxies. This approximation is best where the fraction of uncataloged luminosity is lowest: i.e., where the missing luminosity is dominated by the recorded luminosity. At large distances the opposite is true, and we expect this approximation to be less accurate. Nevertheless, the specific nature of the spatial distribution at these distances is negligible for the initial LIGO, where only small fractions of detections will be due to galaxies at these large distances.

2.3. *The Chirp Mass and Its Distribution*

The GW inspiral signal depends, to leading order, on the so-called chirp mass, denoted $\mathcal{M}$:

$$\mathcal{M} \equiv \mu^{3/5} M^{2/5}, \tag{3}$$

where μ is the system's reduced mass and M its total mass. To complete our specification of the physical BCO population, we must characterize the population distribution with chirp mass.

We model the distribution of BCO systems with component masses using the StarTrack (BKB02) binary synthesis code. We use the resulting chirp mass distribution to determine the signal strength from a given binary at our GW detector. For example, Figure 2 (which also appears in Bulik & Belczynski 2003) shows the distribution of BCO chirp masses, as calculated using the StarTrack binary synthesis code and the BKB02 reference model A. (While we confine attention to reference model A in this section, we explore the dependence of the

[6] Previous work by Lipunov et al. (1995) similarly utilizes the Tully NBG to map the distribution of GW sources. Note that our purpose and analysis greatly diverge from those of this earlier work; our emphasis on selection effects demands different considerations (e.g., knowledge of detector location, orientation, and noise characteristics, correct compensation for incompleteness of galaxies in Tully's NBG and galaxies beyond the range of NBG) and enables us to consider different questions from those in Lipunov et al.

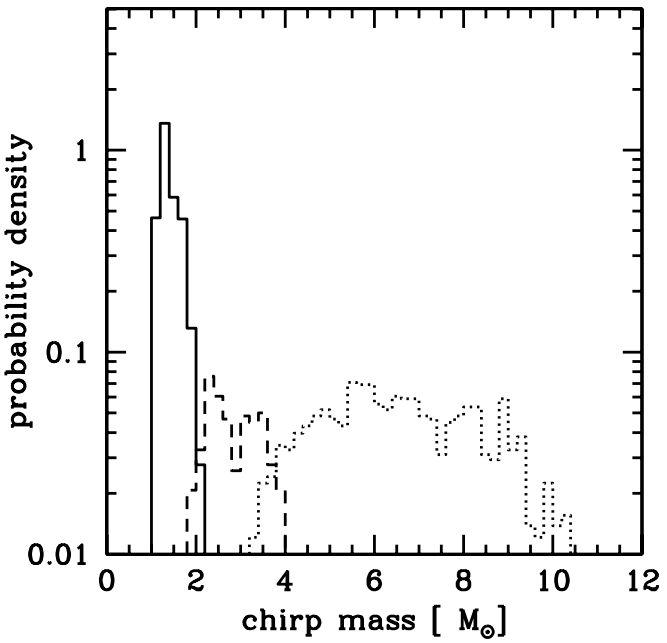

FIG. 2.—Chirp mass distribution for inspiraling binaries, using model A from BKB02: NS-NS (*solid line*), NS-BH (*dashed line*), and BH-BH (*dotted line*).

observed rates and distributions on the full range of BKB02 reference models in § 4.5.)

3. THE DISTRIBUTION OF BCOs ANTICIPATED IN OBSERVATIONS

Here we use the model for the physical BCO population developed in the previous section to determine the observed coalescence rate and distribution as a function of the detector's noise characteristics.

The strength of the BCO inspiral signal observed in a detector system is characterized by the signal-to-noise ratio ρ, which depends on the detector's noise spectrum and the BCO chirp mass, distance, sky position, and orbital inclination. Detected binary systems will have signal-to-noise ratios greater than a threshold ρ_0.

For ground-based GW detectors like LIGO, the signal from a coalescing BCO system persists in the detector for on the order of seconds. Over that period the accumulated signal-to-noise ratio will depend on the detector's noise spectrum, the binary system's distance, orbital plane inclination with respect to the detector's line of sight, and location on the detector's sky, and a function—the so-called chirp mass (see eq. [5a])—of the binary's component masses. The population model described in § 2 thus determines all the parameters necessary to evaluate whether a given binary system will be observed by, e.g., the LIGO detector system.

First predictions for the chirp mass distribution of observed systems were recently obtained by Bulik & Belczynski (2003), who consider varying underlying binary parameters. In addition, Bulik et al. (2004) studied the influence of different cosmological models on the observed chirp mass distribution. Complementing these studies, we determine the distribution of observed systems from the same physical BCO population model; however, we include the effects of anisotropic distribution of galaxies, while we do not consider the different underlying cosmological assumptions. Our method is as follows.

We first draw a representative sample of binary systems populating each galaxy; we evaluate the expected signal-to-noise ratio in the detector system; we determine the observed population by choosing the subset of systems whose signal-to-noise ratio in the detector system is greater than the detection threshold. Throughout this work we assume a signal-to-noise ratio threshold for detection ρ_0 equal to 8. The results presented in this work are based on $\simeq 10^6$ binaries drawn randomly from $\simeq$75,000 galaxies. The ratio of the observed number of systems to the number of systems in the parent population defines the detection efficiency. The rate of detected inspiral events is equal to the merger rate in the physical population, reduced by the detection efficiency.

3.1. *Signal-to-Noise Ratio*

The strength of a signal event observed in a detector is characterized by the event's signal-to-noise ratio ρ. The anticipated ρ-value associated with a particular source depends on the detector, the source, and the method of data analysis. For coalescing BCOs there is an optimal method of analysis—matched filtering—that allows us to express the *anticipated* ρ for a particular binary system in terms of its distance, component masses, and orientation with respect to the detector. Even for identical sources the actual signal-to-noise ratio will vary from instance to instance owing to the stochastic character of detector noise.

The expected ρ-value associated with a BCO observed in a single detector using the technique of matched filtering was first derived by Finn & Chernoff (1993); here we use the particular expression as given in Finn (1996):

$$\rho_D \equiv 8\Theta\left(\frac{r_0}{D}\right)\left(\frac{\mathcal{M}}{1.2\ M_\odot}\right)^{5/6}\zeta(f_{\max}), \tag{4}$$

where

$$\mathcal{M} = \mu^{3/5}M_{\rm tot}^{2/5}, \tag{5a}$$

$$r_0^2 \equiv \frac{5}{192\pi}\left(\frac{3}{20}\right)^{5/3} x_{7/3}\ M_\odot^2, \tag{5b}$$

$$x_{7/3} \equiv \int_0^\infty \frac{df(\pi\ M_\odot)^2}{(\pi f\ M_\odot)^{7/3}S_h(f)}, \tag{5c}$$

$$\zeta(f_{\max}) \equiv \frac{1}{x_{7/3}}\int_0^{2f_{\max}} \frac{df(\pi\ M_\odot)^2}{(\pi f\ M_\odot)^{7/3}S_h(f)}, \tag{5d}$$

D is the luminosity distance to the binary system, Θ is a function of the relative orientation of the binary (including its orbital plane inclination) and the detector, M and μ are the system's total and reduced mass, respectively, $S_h(f)$ is the detector noise power spectral density in units of squared GW strain per Hz, and $f_{\max}$ is the GW frequency at which the inspiral detection template ends (and which is no greater than the frequency at which the inspiral itself transitions into coalescence).

The LIGO detector system consists of not one but three detectors: a 4 km interferometer (H1) and a 2 km interferometer (H2) located near Hanford, Washington, and a 4 km interferometer (L1) located near Livingston, Louisiana. The signal-to-noise ratio associated with any given inspiraling BCO will be different in the three interferometers, owing to differences in their respective noise power spectral densities S_h and their geographic locations and orientations. When we speak of the signal-to-noise ratio associated with a BCO inspiral observed

in LIGO, we assume that these three interferometers are used together as a single detector, following Finn (2001b), in which case the signal-to-noise ratio for the network of three detectors can be approximated, for LIGO, by the quadrature sum of the signal-to-noise ratios in the individual detectors:

$$\rho^2 = \rho_{\rm H1}^2 + \rho_{\rm H2}^2 + \rho_{\rm L1}^2, \quad (6)$$

where $\rho_{\rm H1}$, $\rho_{\rm H2}$, and $\rho_{\rm L1}$ refer to the expected signal to noise of the binary in the H1, H2, and L1 detectors, calculated via equation (4), respectively.

In the following subsections we discuss ζ, $f_{\rm max}$, and Θ in more detail.

3.2. ζ *and* $f_{\rm max}$

The chirp mass $\mathcal{M}$ and frequency $f_{\rm max}$ are intrinsic properties of the BCO. The GW signal from an inspiraling binary system is nearly sinusoidal, with a frequency twice the binary's orbital frequency. Consequently, over time the signal enters the detector's effective bandwidth from low frequency, travels across the band as time elapses, and—if the frequency at which the inspiral ends and coalescence takes place is high enough—leaves the detector's bandwidth at high frequency. The quantity $\zeta(f_{\rm max})$ is unity when the BCO's inspiral phase completely covers the detector's effective bandwidth and is less than unity to the degree that the inspiral terminates within the detector's band or before the signal enters the band.

We model $f_{\rm max}$ by assuming that the BCO inspiral phase proceeds until an innermost circular orbit (ICO) is reached, at which point the components coalesce in less than an orbital period. Using the post-Newtonian approximation, together with a compelling *Ansatz*, Kidder et al. (1993) have estimated the ICO orbital frequency for binaries with components of equal mass to be

$$f_{\rm ICO} = 710\ {\rm Hz}\left(\frac{2.8\ M_\odot}{M}\right). \quad (7)$$

We assume that $f_{\rm max}$ is equal to $f_{\rm ICO}$.

For binaries with unequal-mass components, $f_{\rm ICO}$ depends additionally on a function of μ/M. For the binaries that we encounter in our Monte Carlo procedure (where the mass ratio of the larger to the smaller is rarely above 2.5), the effect of the mass asymmetry is small. We ignore this small correction, making exclusive use of equation (7).

The question of how the transition from inspiral to coalescence takes place is far from settled. The Kidder et al. (1993) calculation of $f_{\rm ICO}$ treats the binary components as point masses, ignores hydrodynamic effects, and employs an *ansatz* that—while compelling—is still a guess, based on an analogy to Schwarzschild spacetime. A number of authors have discussed hydrodynamic effects that may lead to coalescence at orbital frequencies less than $f_{\rm ICO}$ (Faber et al. 2002; Lai & Wiseman 1996; Lai et al. 1994), and numerical simulations of relativistic binary systems have led to other results for the $f_{\rm ICO}$ orbital period (Taniguchi & Gourgoulhon 2002; Grandclément et al. 2002; Cook 2002; Baumgarte & Shapiro 2003). Future work will need to explore the dependence of the observed rates and chirp mass distribution on this uncertainty as well.

3.2.1. *The Antenna Projection* Θ

Interferometric detectors like LIGO are sensitive to a single GW polarization and have a quadrupole antenna pattern (Thorne 1987). The function Θ, defined in detail in Finn & Chernoff (1993) and Finn (1996), describes the dependence of the inspiral signal-to-noise ratio on the position and orientation of the binary relative to the detector. It ranges from 0 to 4, with typical values near unity *when we consider an isotropic distribution of sources*. In the local neighborhood, however, the distribution of galaxies is not isotropic on the detector's sky: e.g., there are significant concentrations of galaxies in the direction of the Virgo and the Fornax Clusters, which are at a fixed declination relative to the LIGO detectors. Since the signal-to-noise ratio of a binary is directly proportional to Θ, binaries from galaxies at some declinations are more likely to be detected than binaries in others, and this plays an important role in relating the observed event rate to the underlying, physical event rate.

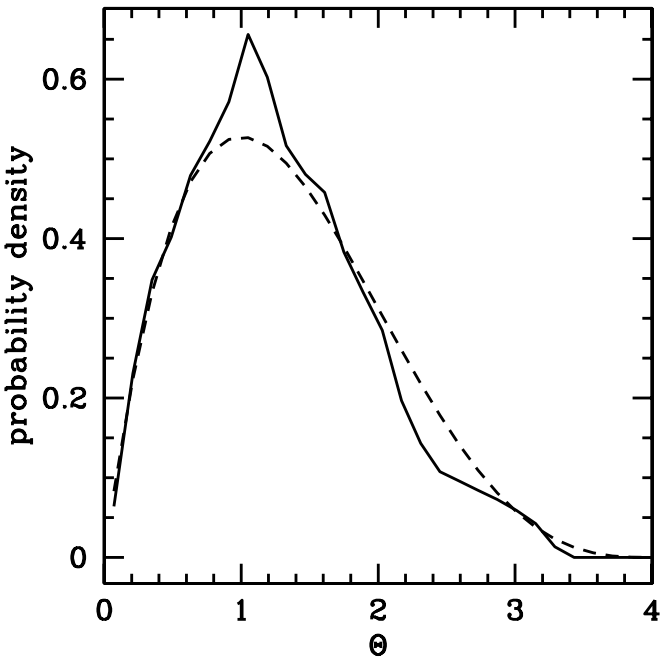

FIG. 3.—Normalized probability distribution of Θ. The solid line shows the distribution for inspirals from galaxies in the Virgo Cluster observed with LIGO Hanford. The dashed line shows the distribution assuming that sources are uniformly distributed in space.

For example, Figure 3 compares the distribution of Θ for binaries associated with Virgo Cluster galaxies (*solid line*), as observed at the LIGO Hanford detector, with that for binaries isotropically distributed about the sky. Note that Virgo is relatively poorly positioned in declination relative to the LIGO Hanford detector, leading to a smaller number of sources with large Θ then we would expect for an isotropic distribution of binaries.

3.3. *The Noise Power Spectral Density,* $S_h(f)$

The influence of the detector on the signal-to-noise ratio ρ enters through the quantity r_0 and the function $\zeta(f)$, each of which depends on the detector's strain-equivalent noise power spectral density $S_h(f)$ (see eqs. [4] and [5]).

A GW signal incident on an interferometric detector like LIGO leads to a response that can be characterized as a projection $h(t)$ of the incident GW strain acting on the detector arms. Measurement noise, which is contributed at many points in the transduction chain, is indistinguishable from a GW signal $h_n(t)$, and we characterize the strain-equivalent noise by its mean square amplitude, $\bar{h}_n^2$. The strain-equivalent noise power spectral density $S_h(f)$ is the contribution to $\bar{h}_n^2$ from

noise components in a 1 Hz bandwidth about the frequency f, so that

$$\bar{h}_n^2 = \int_0^\infty df\, S_h(f). \tag{8}$$

LIGO is currently in the late stages of commissioning, with results from early data sets under review (Abbott et al. 2004a, 2004b, 2004c). When commissioning is complete, the noise power spectral density $S_h(f)$ will meet or exceed the specification given in Lazzarini & Weiss (1996, Fig. 3-2). To evaluate the sensitivity of the initial LIGO instrumentation, we use a parameterized version of this noise curve,

$$S_h(f) = 9 \times 10^{-46}\left[(4.49x)^{-56} + 0.16x^{-4.52} + 0.52 + 0.32x^2\right]\mathrm{Hz}^{-1}, \tag{9}$$

$$x \equiv \frac{f}{150\ \mathrm{Hz}} \tag{10}$$

(B. J. Owen 2001, private communication), for each of the two LIGO 4 km interferometers (referred to as H1 and L1). For the 2 km Hanford detector (referred to as H2), we approximate $S_{h,2\,\mathrm{km}}(f)$ as $4S_{h(f)}$.[7] As a consequence of this approximation, note that for the initial LIGO detectors

1. $\zeta(f_{\max})$ is the same function of $\mathcal{M}$ for the H1, H2, and L1 approximations; and
2. r_0 for H1 and L1 are identical and twice the value appropriate for H2:

$$r_{\mathrm{H1}} = r_{\mathrm{L1}} = 2r_{\mathrm{H2}} = 7.7. \tag{11}$$

The LIGO Laboratory and the LIGO Scientific Collaboration have also recently proposed an advanced set of LIGO detectors. In addition to extending the 2 km Hanford interferometer to a full 4 km, these advanced detectors would have a much lower detector noise and a greater effective bandwidth for BCO inspiral searches. We have also evaluated the event rates and distributions, using the current estimates for the limiting noise sources associated with this advanced detector system (D. Shoemaker 2003, private communication). Figure 4 shows the target noise curve for the initial LIGO detectors (eq. [9]) and the current estimate for the advanced LIGO limiting noise curve. Again note that, as a consequence of this approximation,

1. $\zeta(f_{\max})$ is the same function of $\mathcal{M}$ for the H1, H2, and L1 approximations; and
2. r_0 for H1, H2, and L1 are identical for the advanced LIGO detectors:

$$r_{\mathrm{H1}} = r_{\mathrm{L1}} = r_{\mathrm{H2}} \simeq 120. \tag{12}$$

4. RESULTS

In this section we discuss how the differential sensitivity of the LIGO detectors, as a function of source sky position, chirp mass, distance, and analysis threshold, can be combined with the spatial and chirp mass distribution of coalescing binaries, to determine how the observed coalescing binary distribution reflects the underlying physical distribution.

[7] Not all noise sources scale with length in a simple manner: in particular, the laser shot noise spectrum depends on the Fabry-Pérot arm cavities in a more complicated manner. Nevertheless, this approximation is more than suitable for our purpose here.

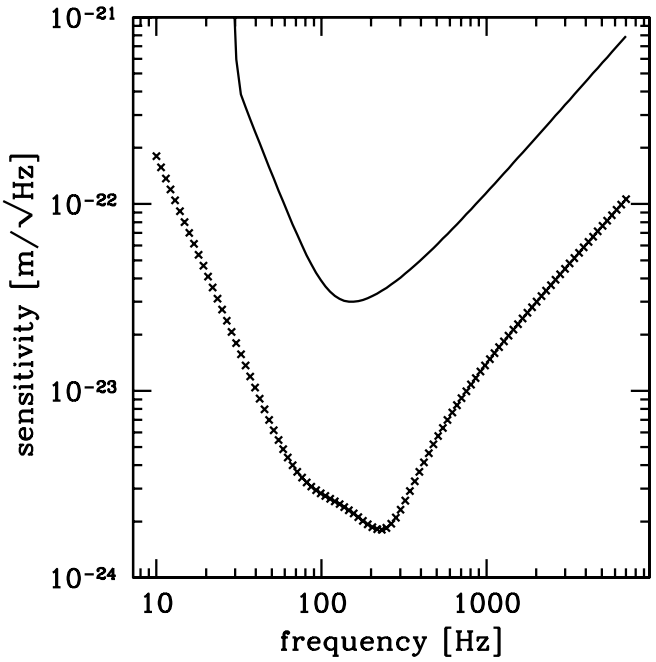

FIG. 4.—Target noise curves for initial (*solid line*) and advanced (*crosses*) LIGO detectors.

4.1. *BCO Populations in Galaxies*

In addition to its dependence on distance, sky position, and orbital plane inclination, the sensitivity of GW detectors like LIGO to a particular BCO depends on a function of the binary's component masses. We use the BKB02 binary synthesis calculations to populate each galaxy with a distribution of binary systems of different chirp mass.[8] The luminosity scaling of Phinney (1991) is naturally applicable to our approach, and we set the total inspiral rate for a particular galaxy equal to the Milky Way rate $R_{\mathrm{det,\,MW}}$ times its blue luminosity (corrected for reddening) in units of the Milky Way blue luminosity. Note that $R_{\mathrm{det,\,MW}} = R_{\mathrm{MW}}$, since the initial LIGO detectors are expected to detect essentially all BCO inspirals in the Milky Way with chirp mass less than 18 $M_\odot$ (which exceeds the typical expected maximum chirp mass; see Fig. 2):

$$\mathcal{R}_{\mathrm{gal}} = \frac{L_{\mathrm{gal},\,b}}{L_{\mathrm{MW}}} R_{\mathrm{MW}}. \tag{13}$$

Our principal tool for understanding how the physical distribution of coalescing binaries is reflected in the observed distribution is the detection efficiency. We define the detection efficiency as the fraction of binaries from a given population that are detected with a signal-to-noise ratio higher than a chosen threshold (in this study 8). We may thus consider the detection efficiency for all binaries in a given galaxy, or the efficiency for NS-NS binaries over all galaxies, or the efficiency for detection of binaries at a given sidereal time, etc.

Under the assumption of uniform galaxy distribution, the natural measure of a detector's sensitivity is the volume of space surveyed, which is conveniently expressed as an effective radius r such that the surveyed volume is equal to the volume of

[8] For most of § 4, we confine our attention to reference model A from BKB02. However, we explore the full set of BKB02 models in § 4.5.

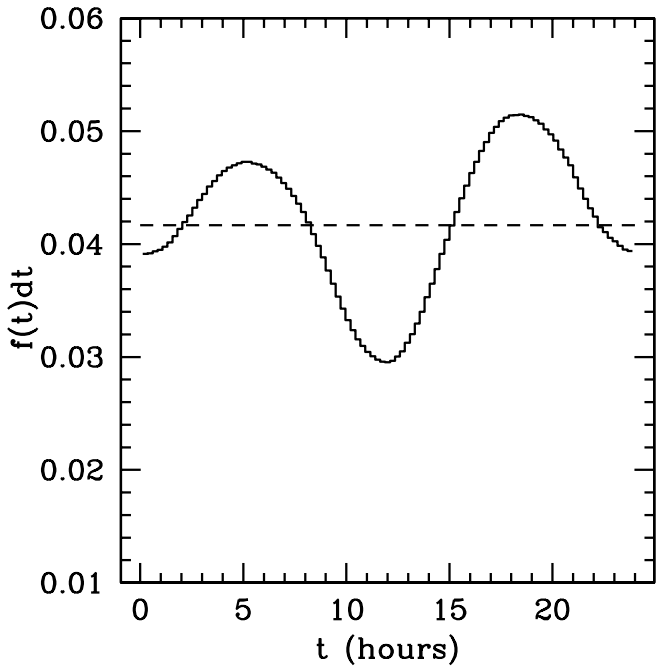

FIG. 5.—Probability $f(t)\,dt$ that an initial LIGO detection would come at an hour t during the day. Here t is the UT plus the sidereal time at Greenwich at 0 h UT. The probability assuming uniform spatial distribution of galaxies is given for comparison (*dashed line*).

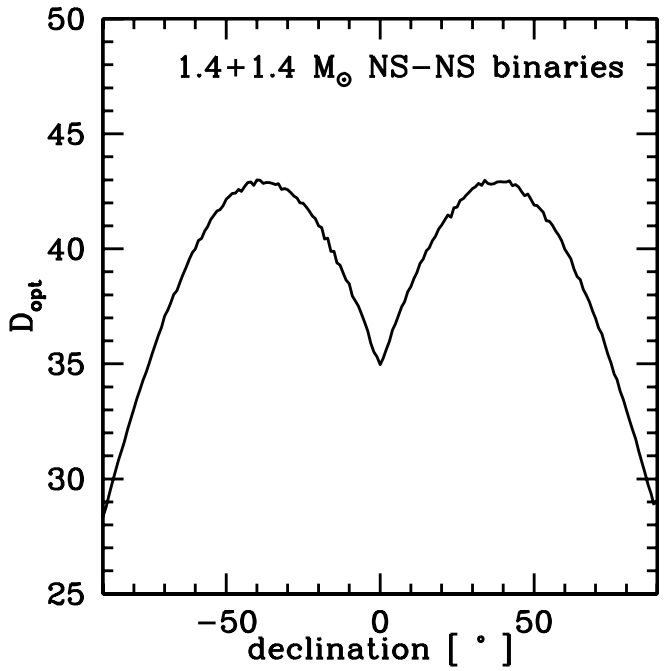

FIG. 6.—Maximum detection distance for the most optimally positioned binary as a function of declination. LIGO Hanford and LIGO Livingston have latitudes of $\simeq 45^\circ$ and $\simeq 30^\circ$, respectively. The peak in this plot corresponds to sources overhead at a latitude in between the detectors, weighted more toward Hanford, because of its two interferometers vs. Livingston's one.

a sphere of radius r (Finn 2001a). When the actual galaxy distribution and the variation in binary populations among galaxies are taken into account, a different measure of sensitivity suggests itself: the effective number of Milky Way galaxies surveyed,

$$N_G \equiv \frac{R_{\rm det}}{R_{\rm MW}} = \sum_i \frac{L_i}{L_{\rm MW}} f_{{\rm det},\,i}, \tag{14}$$

where $f_{{\rm det},\,i}$ is the detection efficiency and L_i is the blue luminosity for galaxy i, $L_{\rm MW}$ is the Milky Way's blue luminosity, and $L_i/L_{\rm MW}$ is the blue luminosity scaling, as discussed in § 2.2. The concept of N_G is more appropriate for our approach, since it takes into account the actual galaxy distribution and the BCO mass distribution. As detectors become more sensitive, N_G grows accordingly.

In this formulation $R_{\rm det} = N_G R_{\rm MW}$. The Galactic inspiral rate $R_{\rm MW}$ can be calculated based on the current observed sample of NS-NS binaries (Kalogera et al. 2004) and from population synthesis calculations (e.g., BKB02).

4.2. *Detection Efficiency and Sidereal Time*

Interferometric detectors like LIGO are most sensitive to GWs of a single polarization incident normal to the plane of the detector's arms. As the Earth rotates about its axis, the sky locations and polarization of sources to which it is most sensitive rotate as well. Since galaxies are not uniformly distributed about the sky, the expected rate of detected coalescence events is periodic with the sidereal day. The detailed variation depends on the geographical distribution of galaxies, the distribution of coalescing binaries with system chirp mass, and the signal-to-noise ratio threshold for detection. Figure 5 shows the probability density for detections under the assumptions that the geographical distribution of galaxies is determined by our galaxy catalog approach (see § 2.2.1), that the chirp mass distribution of coalescing binaries is given by BKB02 model A, and that the signal-to-noise ratio threshold for detection in the initial LIGO ρ_0 is 8. Here time t is measured in hours and is given by the UT plus the sidereal time at Greenwich at 00h UT. The Virgo Cluster is above a point between the Hanford and Livingston detectors for approximately the duration 18 hr $< t <$ 20 hr, closely coinciding with the peak in Figure 5.

4.3. *Dependence of Detection Range and Efficiency on Declination*

Setting aside the actual distribution of galaxies, it is interesting to note the dependence of the detector's "range"—or distance to the most distant observable source above the threshold—on source sky position. When sampled over sidereal time, the range depends on the sky position only through declination. Figure 6 shows, for the initial LIGO, the detector range as a function of declination, normalized to $1.4 + 1.4\,M_\odot$ NS-NS binaries. For an advanced LIGO with the H2 interferometer extended to 4 km, the declinations of maximum range will shift slightly toward the zenith and nadir of L1.

Figure 7 shows the dependence of detection efficiency—i.e., the fraction of binaries detected—on declination for galaxies at the distance of the Virgo Cluster. Note that this dependence on declination will change if the ground-based detectors are located differently. In particular, the sensitivity of detectors to inspirals from the Virgo Cluster improves for detectors with latitudes corresponding to declinations near that of Virgo. Indeed, Livingston and VIRGO, because of the relative proximity of their latitude and the Virgo Cluster's declination, are more optimally placed relative to the Virgo Cluster than the Hanford or GEO detectors. Interestingly, had H1 and H2 been constructed exactly as they are, but instead at the present latitude of the VIRGO detector, the LIGO network would detect

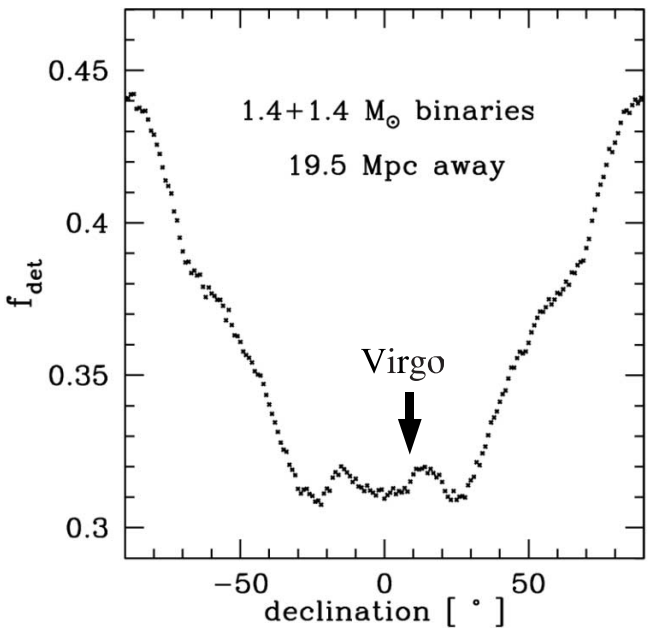

FIG. 7.—Detection efficiency as a function of declination, for $1.4 + 1.4\ M_{\odot}$ NS-NS binaries. Here $f_{\rm det}$ is attenuated in regions near the equatorial plane, including the Virgo Cluster, which is a major source of NS-NS detections.

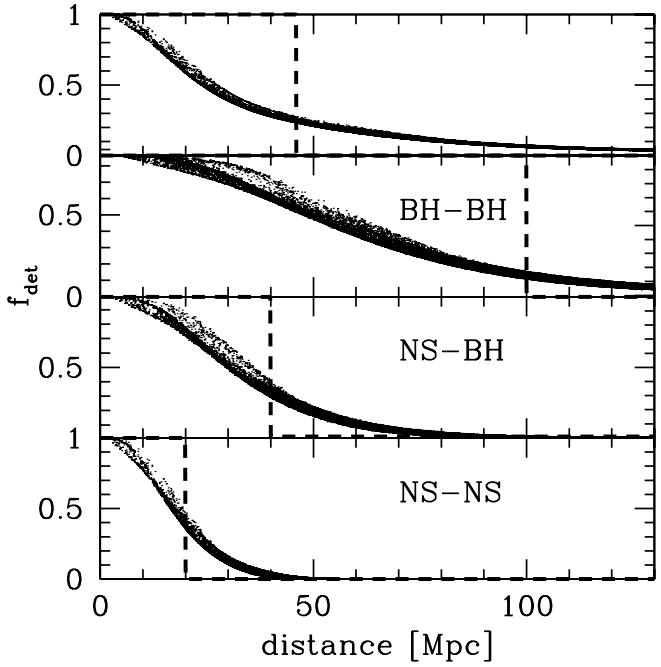

FIG. 8.—Detection efficiency of every galaxy in our catalog, as a function of galaxy distance. *Top*: Total efficiency for the complete population of binaries. Subsequent panels shows the efficiencies for the BH-BH, NS-BH, and NS-NS subpopulations for initial LIGO. Previous studies adopted a steplike detection efficiency for initial LIGO at 20 Mpc for NS-NS, 40 Mpc for NS-BH, 100 Mpc for BH-BH, and 46 Mpc for the entire population: these cutoffs are shown as vertical dashed lines.

about 25% more NS-NS inspirals (at design sensitivity) from the Virgo Cluster.

Note that the maximum detection efficiency at this distance in Figure 7 occurs for galaxies located at the celestial poles. This might be surprising, since the detectors are most sensitive to sources at their zenith or nadir. The reason for this apparently paradoxical result is that a galaxy at a declination corresponding to the detector's latitude is only at the detector's zenith for a short fraction of a sidereal day, while the efficiency for galaxies at a celestial pole is independent of sidereal time. Despite the shorter duty cycle for sources at the detector's zenith or nadir, it is still the case that galaxies at these locations will be seen to greater distances.

4.4. *Dependence of Detection Efficiency on Both Galaxy and BCO Mass Distributions*

Figure 8 shows the detection efficiency of every galaxy in our catalog, plotted as a function of galaxy distance. The top panel shows the total efficiency for the complete population of binaries. Subsequent panels shows the efficiencies for the BH-BH, NS-BH, and NS-NS subpopulations for the initial LIGO. Galaxies at a given distance have a range of efficiencies owing to their different declinations. This may amount to as much as a 40% variation.

Previous studies adopted a detection efficiency for the initial LIGO of unity up to distances of 20 Mpc for NS-NS, 40 Mpc for NS-BH, 100 Mpc for BH-BH, and 46 Mpc for the entire population, and zero beyond. These cutoffs are shown as vertical dashed lines in Figure 8. In our more realistic approach, one sees nonzero efficiencies to much greater distances. For example, BH-BH binaries are observed with 10% efficiency even at distances of 130 Mpc. On the other hand, inside the previously adopted cutoff distances, the efficiency is not 100%: for example, the overall efficiency for Virgo Cluster inspirals is 60%.

The NS-NS, NS-BH, and BH-BH subpopulation efficiencies vary differently with distance owing to their different chirp mass distributions. Figure 9 shows the expected distribution with chirp mass of detected binaries. This should be contrasted with the actual population distribution, as shown in Figure 2. As expected, the distribution is dominated by BH-BH binaries; however, the relative proportion of detected

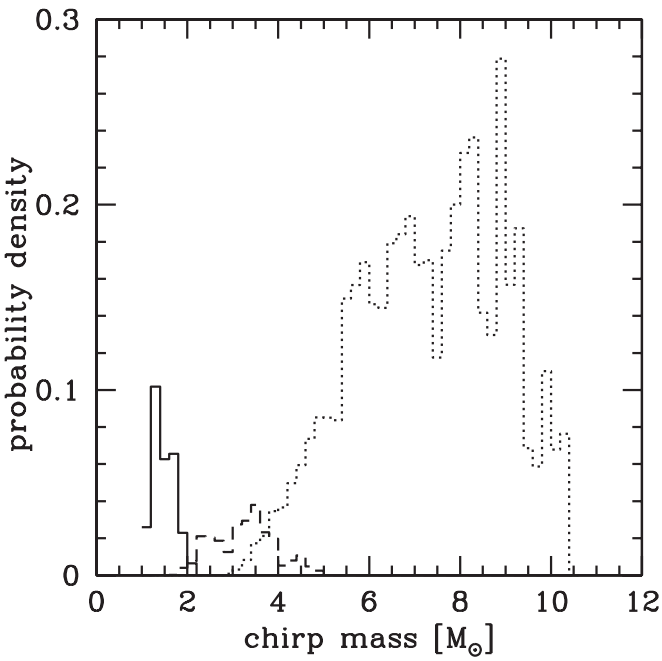

FIG. 9.—Expected normalized chirp mass distribution for detected inspirals, using model A from BKB02: NS-NS (*solid line*), NS-BH (*dashed line*), and BH-BH binaries (*dotted line*). Compare to the intrinsic chirp mass distribution in Fig. 2.

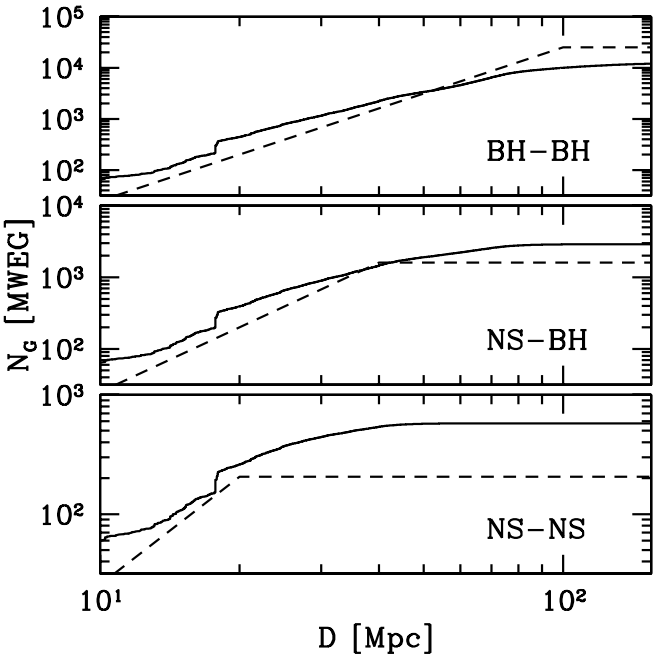

FIG. 10.—Effective number of MWEGs surveyed by initial LIGO, for events within a distance D for BH-BH (*top*), NS-BH (*middle*), and NS-NS (*bottom*) binaries. The dashed curves are calculated using the uniform approach adopting maximum detection distances for NS-NS, NS-BH, and BH-BH of 20, 40, and 100 Mpc, respectively. The solid curves are calculated using the galaxy catalog approach.

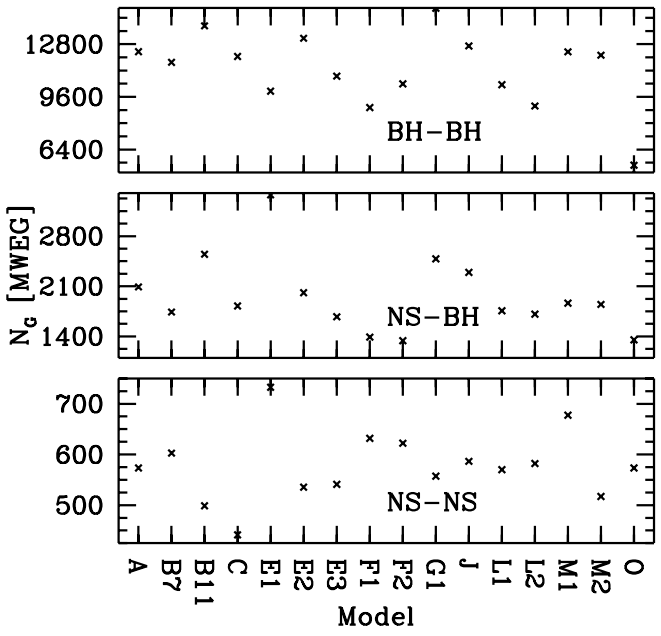

FIG. 11.—Plots of N_G for different population synthesis models.

NS-NS binaries is more than double the proportion previously calculated assuming a uniform galaxy distribution (Bulik & Belczynski 2003). The increased proportion of NS-NS relative to BH-BH binaries arises because the uniform galaxy distribution assumption significantly underestimates the number of galaxies in the nearby universe. As is apparent from Figure 1, this underestimate is greater at Virgo Cluster distances, where there is still significant efficiency for NS-NS binaries, than at, e.g., 100 Mpc, where only BH-BH binaries are detected. Correspondingly, the boost in the number of NS-NS binaries, relative to the uniform distribution model, is greater for NS-NS binaries than it is for BH-NS and BH-BH binaries. (The sensitivity of the advanced LIGO detectors is sufficiently great that the uniform assumption is applicable and the distribution of detected sources will follow Bulik & Belczynski 2003 more closely.) From Figure 9 we also note that about half the detected binaries are expected to have chirp masses in the range 5–9 $M_\odot$, with a peak at 9 $M_\odot$ (corresponding to two 10 $M_\odot$ BHs). These results can be folded with the most current Galactic rate estimates to estimate the number of BH inspiral events with chirp masses in the above range that we might expect from initial LIGO observations in one year at full sensitivity. It is clear that data searches would need to focus on these higher masses, at which, however, the GW wave forms are harder to calculate. Nevertheless, an effort focusing on these systems is necessary, since limits in this range will be most constraining to population models.

4.5. *Effective Number of Milky Way Equivalent Galaxies (MWEGs) Surveyed*

The naive use of an effective radius can lead to a misunderstanding in the overall rate and nature of detected coalescing binary systems. Figure 10 shows the cumulative rate of detections by the initial LIGO detector from sources within a distance D. The dashed line shows the cumulative rate, assuming a uniform distribution of galaxies and a 100% efficiency for binaries within a distance r, with r equal to 20, 40, and 100 Mpc for NS-NS, NS-BH, and BH-BH binaries, respectively. The solid line shows the approach taken here: i.e., the rate of detected binaries within a distance D, taking into account the actual galaxy distribution, the estimated number of binaries per galaxy, the distribution of binaries with chirp mass, and the overall detection efficiency for each galaxy. The solid lines show evidence that particular geographic features in the distribution of galaxies have sharp effects on rate of detection. The most striking example is the Virgo Cluster (the spike at 20 Mpc), which comprises, for example, 20% of NS-NS detections. In general, NS-NS extrapolation factors based on the uniform galaxy density assumption have been underestimated by a factor of $\simeq$2–3, while BH-BH extrapolation factors have been slightly overestimated, by a factor of less than 100%.

Even though the quantity N_G is normalized to the Galactic rate, it still depends on the assumed model chirp mass distribution. To examine this dependence, we consider all models calculated in BKB02 that are considered realistic at present. We calculate the associated N_G values for each of the three BCO populations shown in Figure 11. These models differ in terms of a number of parameters that determine single-star and binary evolution (e.g., stellar winds, common envelope evolution, NS and BH kicks; for a detailed discussion see BKB02). On the basis of these models it is evident that the variation in N_G is lower than a factor of 1.5–2 for the three types of BCO populations. We consider these variations to represent the systematic uncertainty associated with the extrapolation factor N_G.

Finally, we explore the growth of N_G with detector sensitivity. As LIGO's sensitivity improves, approaching design sensitivity for the initial and advanced detectors, of particular interest is the growth of N_G for NS-NS binaries. In lieu of a detection, N_G is important for assessing upper rate limits for NS-NS inspirals in the Milky Way. A measure of the sensitivity

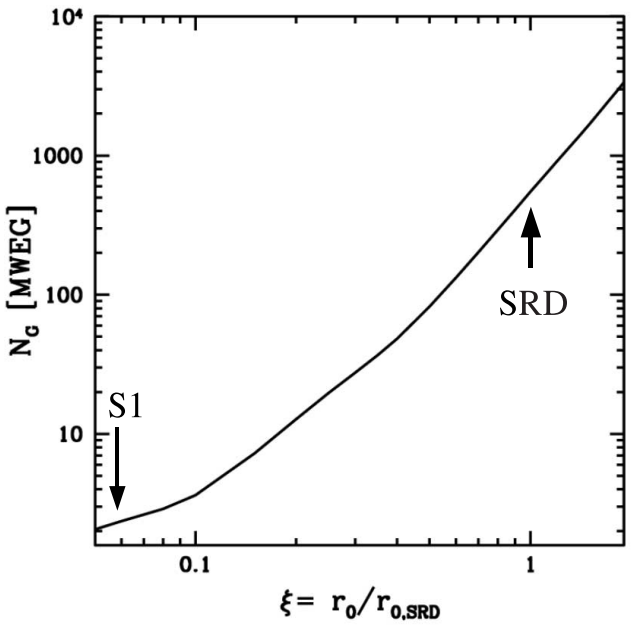

FIG. 12.—Effective number of MWEGs surveyed by LIGO as a function of detector sensitivity ξ normalized to the initial LIGO design sensitivity for NS-NS binaries. The arrow on the left denotes the instrument sensitivity achieved during the first science run.

improvement is the increase of the value of r_0 (see eq. [5c]) or the ratio

$$\xi \equiv \frac{r_0}{r_{0,\,\mathrm{SRD}}}, \tag{15}$$

where $r_{0,\,\mathrm{SRD}}$ is calculated similarly to r_0, but with the advanced LIGO noise curve. In Figure 12, we show the dependence of N_G on ξ for the initial LIGO configuration of 4 and 2 km detectors at Hanford and a 4 km detector at Livingston. The effective number of MWEGs surveyed increases as x^P, initially with $P < 1$, but with $P \simeq 2.6$ as design sensitivity is reached. This rate represents an increase by a factor of $\simeq$300 MWEGs, compared to the sensitivity of the detectors during the first science run (Abbott et al. 2004a).

5. CONCLUSIONS

In anticipation of the development of GW astrophysics in the next several years, we consider the effects of observational selection effects on the detectability of BCO inspiral events. Our primary goal is to develop a realistic framework for the astrophysical interpretation of rate constraints (from upper limits or inspiral detections) anticipated in the next few years. This interpretation should account for the main selection effects associated with ground-based GW observations and properly constrain models of radio pulsar and BCO populations. As a result of our calculations, we also make realistic estimates for the extrapolation of Galactic inspiral detection rates based on the known spatial distribution of galaxies in the nearby universe and the expected mass distributions of BCOs.

Our results are summarized as follows:

1. The local distribution of galaxies most relevant to NS-NS detections with the initial LIGO is in fact very different from isotropic in sky direction and volume density. Most importantly, the Virgo Cluster represents a significant step in the cumulative blue luminosity (or the cumulative number of MWEGs), all concentrated at a given (rather unfortunate) sky position. Failure to properly account for this local distribution of BCO sources would lead us to underestimate the importance of an upper limit on the inspiral rate derived from GW observations.

2. Until this study, because of the assumption of isotropic distribution of galaxies, detection rates of NS-NS inspirals have been underestimated by factors of 2–4, and those of BH-BH inspirals have been overestimated by nearly a factor of 2. These factors include the systematic uncertainties due to the chirp mass distributions, which are not very well constrained.

3. Detections of inspiral events and measurements of compact object masses are expected to provide us with tighter constraints on the BCO mass distributions and thus on the physics of BCO formation. However, our analysis shows that mass distributions of detected BCOs are strongly skewed toward higher masses (because of their stronger signals), compared to the parent mass distribution (see Figs. 2 and 9). For our reference population model, we find that about half of the detected inspirals correspond to binaries with high chirp masses (5–9 $M_\odot$). Since event rate limits in this range will be most constraining to BCO models, it is evident that there is a need for the development of efficient search methods for such massive systems. Understanding the systematics of this bias will be crucial for the astrophysical interpretation of such detections.

4. Inspiral detection efficiency depends strongly on the host galaxy sky position and the binary orbit orientation with respect to the detectors; as a result, the true maximum distance for an optimally oriented binary can exceed the average detection distance by more than a factor of 2.

5. Using the currently most favorable (at peak probability) estimates of NS-NS inspiral rates for the Galaxy (Kalogera et al. 2004) and our results on N_G values, we find expected initial LIGO detection rates in the range of one event per 3–200 yr (for the reference pulsar population model at 95% confidence level, the range is one event per 3–50 yr).

Of the various galaxy physical properties, we have considered the blue luminosity (corrected for reddening), but we have ignored galaxy metallicity and star formation history. Both of these factors affect the expected mass distribution of BCOs, as well as their birth rate, for a given luminosity. For example, metallicity affects massive stellar winds and the final compact object masses. This effect has already been taken into account in Abbott et al. (2004c), where the Magellanic Clouds have been observed by LIGO. In principle, we would like to include these effects in our calculations (to the extent of our current understanding of binary evolution and how it is affected by these factors); however, at present it does not seem possible, since this information is not available in detail for every galaxy in the catalogs, and we chose to ignore these factors instead of include them for only a very small subset of sample.

With the work presented here we also advance a paradigm for using initial LIGO binary inspirals to constrain models of binary evolution and BCO formation and of pulsar population properties. Using the current estimates of NS-NS inspiral rates in MWEGs (Kalogera et al. 2004) and scaling to the BH-BH population, it is clear that LIGO should eventually provide an astrophysically significant bound on the rate of BH-BH inspirals in the nearby universe. In the context of a particular binary synthesis model, such a bound can be translated to a bound on the MWEG BH-BH inspiral rate, as well as on the rate for the NS-NS and NS-BH subpopulations.

The derived bound on the NS-NS subpopulation can be compared to the estimates that arise from binary pulsar observations (Kalogera et al. 2004). Note that GW observations may also directly bound the coalescence rate for the NS-BH and NS-NS subpopulations at a significant level. All these bounds will be consistent only for certain binary formation and synthesis models. In this way, GW observations will contribute to our understanding of compact binary formation and evolution.

This work is partially supported by National Science Foundation awards PHY 01-21420 (V. K.), PHY 00-9959 (L. S. F.), and PHY 01-14375 (L. S. F., P. N., and V. K.), and a David and Lucile Packard Science & Engineering Fellowship (V. K.). K. B. acknowledges support of the grant PBZ-KBN-054/P03/2001. P. N. and V. K. are also grateful for the warm hospitality of the Center for Gravitational Wave Physics at Penn State. The Center for Gravitational Wave Physics is funded by the NSF under cooperative agreement PHY 01-14375.

REFERENCES

Abbott, B., et al. 2004a, Nucl. Instrum. Methods Phys. Res. A, 517, 154
———. 2004b, Phys. Rev. D, 69, 082004
———. 2004c, Phys. Rev. D, 69, 122001
Amaldi, E., Cosmelli, C., Pallottino, G. V., Pizzella, G., & Rapagnani, P. 1986, Nuovo Cimento C, 9, 829
Ando, M., et al. 2001, Phys. Rev. Lett., 86, 3950
Astone, P., et al. 1993, Phys. Rev. D, 47, 362
———. 1997, Astropart. Phys., 7, 231
Baumgarte, T. W., & Shapiro, S. L. 2003, Phys. Rep., 376, 41
Belczynski, K., Kalogera, V., & Bulik, T. 2002, ApJ, 572, 407 (BKB02)
Bulik, T., & Belczynski, K. 2003, ApJ, 589, L37
Bulik, T., Belczynski, K., & Rudak, B. 2004, A&A, 415, 407
Burgay, M., et al. 2004, Nature, 426, 531
Caron, B., et al. 1997, Nucl. Phys. B, 54, 167
Cook, G. B. 2002, Phys. Rev. D, 65, 084003
Faber, J. A., Grandclément, P., Rasio, F. A., & Taniguchi, K. 2002, Phys. Rev. Lett., 89, 231102
Finn, L. S. 1996, Phys. Rev. D, 53, 2878
———. 2001a, in AIP Conf. Proc. 575, Astrophysical Sources for Ground-based Gravitational Wave Detectors, ed. J. M. Centella (Melville, NY: AIP), 92
———. 2001b, Phys. Rev. D, 63, 102001
Finn, L. S., & Chernoff, D. F. 1993, Phys. Rev. D, 47, 2198
Grandclément, P., Gourgoulhon, E., & Bonazzola, S. 2002, Phys. Rev. D, 65, 044021
Hulse, R. A., & Taylor, J. H. 1974, ApJ, 191, L59
Kalogera, V., Narayan, R., Spergel, D. N., & Taylor, J. H. 2001, ApJ, 556, 340
Kalogera, V., et al. 2004, ApJ, 601, L179
Kidder, L. E., Will, C. M., & Wiseman, A. G. 1993, Phys. Rev. D, 47, 3281
Lai, D., Rasio, F. A., & Shapiro, S. L. 1994, ApJ, 420, 811
Lai, D., & Wiseman, A. G. 1996, Phys. Rev. D, 54, 3958
Lazzarini, A., & Weiss, R. 1996, LIGO Science Requirements Document (SRD), Internal LIGO Document E950018-02-E (Pasadena: Caltech)
Lipunov, V. M., Nazin, S. N., Panchenko, I. E., Postnov, K. A., & Prokhorov, M. E. 1995, A&A, 298, 677
Mauceli, E., Geng, Z. K., Hamilton, W. O., Johnson, W. W., Merkowitz, S., Morse, A., Price, B., & Solomonson, N. 1996, Phys. Rev. D, 54, 1264
Paturel, G., Fouqué, P., Bottinelli, L., & Gouguenheim, L. 1989, A&AS, 80, 299
Phinney, E. S. 1991, ApJ, 380, L17
Prodi, G. A., et al. 1998, in Proc. Second Edoardo Amaldi Con. on Gravitational Waves, ed. E. Coccia, G. Veneziano, & G. Pizzella (Singapore: World Scientific Press), 148
Taniguchi, K., & Gourgoulhon, E. 2002, Phys. Rev. D, 66, 104019
Taylor, J. H., & Weisberg, J. M. 1989, ApJ, 345, 434
Thorne, K. S. 1987, in 300 Years of Gravitation, ed. S. W. Hawking & W. Israel (Cambridge: Cambridge Univ. Press), 330
Tully, R. B. 1988a, Nearby Galaxy Catalog (Cambridge: Cambridge Univ. Press)
———. 1988b, AJ, 96, 73
York, D. G., et al. 2000, AJ, 120, 1579